

國立臺灣大學生命科學院生命科學系



學士班學生論文

Department of Life Science

College of Life Science

National Taiwan University

Bachelor Thesis

運用 CRISPR/Cas9 技術探討 Kv4.2 通道剔除對海馬迴

CA1 錐狀神經元的影響

Effect of Kv4.2 Knockout on Hippocampal CA1

Pyramidal Neurons using Viral CRISPR/Cas9 System

賴品寰

Pin-Huan Lai

指導教授：閔明源 博士

Advisor: Ming-Yuan Min, Ph.D.

中華民國 111 年 4 月

April 2022

誌謝

感謝中研院沈哲鯤院士提供 CaMKII-cre 品系實驗小鼠，以及台大腦心所黃憲松教授協助轉移該鼠到我們實驗室。


非常感謝閔明源老師的用心指導，讓我在進實驗室的這兩年多來學會了非常多的知識與實驗技術。也感謝老師在我實驗進度緩慢時沒有急於催促，而是給予我信心與鼓勵，讓我能沉下心來，腳踏實地的累積 data。能在這麼一個友愛和諧的環境中進行研究，我感到非常的幸運。

感謝實驗室的各位學長姐們在實驗過程中給予我的支持。感謝洪瑋辰學長教導我種種實驗技術，並在我時不時帶著問題打擾的時候都能很有耐心地替我解惑。另外也感謝學長維持實驗室正常運作，讓我們能避免很多需要充足經驗才能避開的麻煩；感謝詹鎬學長維持 rig1 環境，並在實驗疲累之餘願意與我聊天，並給予我許多實驗上的建議；感謝張筠學姊拿娃娃帶給實驗室幸運並讓大家能獲得治癒。感謝實驗室的大家在我完成學士論文的路上給予我的種種協助。沒有你們，我的實驗無法那麼順利的進行。

感謝科技部大專生計畫的經費支持，這帶給我更多的餘裕去選擇品質更好的實驗方法；感謝台大生命科學系提供的資源，給了我許多值得去努力的目標。這些挑戰確實帶给了我許多的進步。

最後，感謝父母在我實驗路上的一路支持。你們總是給予我足夠的信心，讓我能自由的去做我想做的事。沒有你們，我沒有辦法全心全意地走在探索真理的路上。

中文摘要



A 型電閘式鉀離子通道在神經系統中扮演多種角色，包含調節神經興奮性、快速放電與神經傳遞物質釋放。然而過去以基因轉殖小鼠對這些通道進行的研究無法讓我們揭露他們在特定腦區的功能與避免發育代償效應等副作用。為了解決這兩個問題，我們發展了一套以常間回文重複序列叢集關聯蛋白(clustered, regularly interspaced, short palindromic repeats ,CRISPR/Cas9)設計，能在成鼠中執行特定腦區中 Kv4.2 這種 A 型鉀離子通道剔除的系統。陳景萃小姐於台大生科系碩士論文研究中建立此系統，並已初步用免疫組織染色證實其效力。本篇論文進一步以電生理方法證實其有效性。表現 Kv4.2 剔除系統的海馬迴 CA1 錐形細胞展現出的 A 型鉀離子電流顯著降低。此結果顯示陳小姐設計的 Kv4.2 剔除系統可以穩定的在成鼠特定腦區中執行 Kv4.2 的剔除。

關鍵字: A 型鉀離子通道、常間回文重複序列叢集關聯蛋白、海馬迴、免疫組織染色、電生理

Abstract



A-type voltage-gated potassium channels serve numerous functions in neural system, including the regulation of excitability, fast-spiking, and neurotransmitter release. Previous studies of these channels conducted with transgenic mice, however, are unable to uncover their function in specific brain region and prevent unwanted developmental effect. To resolve these problems, in her master thesis works submitted to the Department of Life Science at National Taiwan University, Ching-Tsuey Chen had developed a CRISPR-mediated knockout system which can conduct site-specific gene-editing in adult mouse on an A-type potassium channel – Kv4.2. The knockout system has been proved effective by immunohistochemistry. Here I provide further evidence of its effectiveness by electrophysiology. Pyramidal neurons in hippocampal CA1 region expressing Kv4.2 knockout system exhibited reduced A-type potassium current. This result shows that Kv4.2 knockout system designed by Miss Chen can steadily conduct Kv4.2 knockout in specific region of adult mouse.

Keywords: A-type potassium channels, clustered regularly interspaced short palindromic repeats (CRISPR)/Cas9 system, hippocampus, immunohistochemistry, electrophysiology.

Content

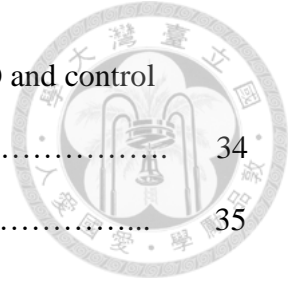


誌謝.....	i
中文摘要.....	ii
Abstract	iii
Content	iv
Chapter 1.Introduction	1
1.1 A-type potassium channels.....	1
1.1.1 Potassium channels.....	1
1.1.2 Voltage-gated potassium channels	1
1.1.3 A-type potassium channels	2
1.2 Kv4.2	3
1.2.1 Overview	3
1.2.2 Distribution of Kv4.2	3
1.2.3 Functional role of Kv4.2	5
1.2.4 Transgenic mice in Kv4.2 research	5
1.2.5 The need of site specific KO in adult in Kv4.2 research	6
1.3 Aim of this study	7
Chapter 2. Materials and Methods	8
2.1 Animals	8
2.2 Virus	8
2.3 Stereotaxic surgery	9
2.4 Preparation of hippocampal slices	10
2.5 Whole-cell clamp recording	10
2.6 Immunohistochemistry	13
2.6.1 Perfusion	13



2.6.2 IHC for Kv4.2	13
2.6.3 Post hoc biocytin histochemistry	14
2.7 Confocal imaging	14
Chapter 3. Results	15
3.1 IHC examination of Kv4.2 KO with CRISPR/Cas9 method in adult hippocampus	15
3.2 A-type potassium current characterization	16
3.3 Kv4.2 KO in hippocampal CA1 pyramidal neurons leads to decreased A-type potassium currents	17
Chapter 4. Discussion	20
4.1 Overview	20
4.2 Effect of site-specific Kv4.2 KO in adult on Kv4.2 expression pattern..	20
4.3 Effect of site-specific Kv4.2 KO in adult on A-type potassium current..	21
4.4 Methodology Considerations	22
Chapter 5. Reference	24
Chapter 6. Figures	28
Figure 1. Genomic editing of Kv4.2 by Kv4.2 KO system.....	28
Figure 2. Genomic editing of Kv4.2 by Kv4.2 control virus system infection.	29
Figure 3. Reversal potential and recovery time of fast-activating potassium channels.	30
Figure 4. Activation and inactivation of fast-activating potassium channels...	31
Figure 5. Recordings from, and post-hoc examination of, Kv4.2 KO or CTRL virus group of CA1 pyramidal neurons	32
Figure 6. Recordings from, and post-hoc examination of, Kv4.2 CTRL group of CA1 pyramidal neurons.....	33

Figure 7. Depolarization induced outward currents of Kv4.2 KO and control groups in CA1 pyramidal neurons.....	34
Figure 8. The I_A are attenuated in Kv4.2 KO group.....	35



Chapter 1. Introduction



1.1 A type potassium channels

1.1.1 Potassium channels

Potassium channels are tetrameric integral membrane proteins that form aqueous pores through which K^+ can flow. They are found in virtually all types of cells in all organisms (Miller, 2000). All K^+ channels carry out a single basic function: the formation of a transmembrane 'leak' extremely specific for K^+ ions. Since cells in an organism's body universally maintain cytoplasmic K^+ concentrations much higher than those extracellularly, opening of a K^+ channel automatically implies a negative-going change in electrical voltage across the cell membrane. This 'membrane hyperpolarization', an electrophysiological jargon, occurs in different physiological contexts for varied purposes (Choe, 2002). There are two broad classes of K^+ channels defined by the transmembrane topology, as reflected in primary sequence: the six-transmembrane-helix voltage-gated (Kv) and the two-transmembrane-helix inward-rectifier (Kir) subtypes (Kuang et al., 2015; Guidelli, 2020).

1.1.2 Voltage-gated potassium channels

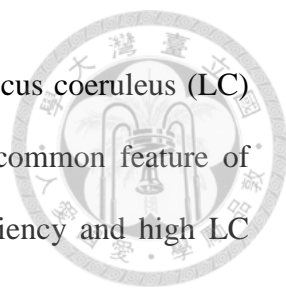
Kv channels can open or close their pores by sensing changes in the transmembrane voltage. Voltage-gated K^+ channels are tetrameric ion channels, as they consist of four identical or homologous units and, with each unit being composed of six transmembrane α -helices (S1–S6) and a p-loop sequence of highly conserved sequence (glycine-tyrosine- glycine or glycine-phenylalanine-glycine) between S5 and S6 transmembrane helices. The four repeated units (I–IV) are circularly arranged with the p-loop face centrally to form the ion pore and function as a K^+ ion selectivity filter (Coetzee et al., 1999; Heginbotham et al., 1994; Kim, and Nimigeon, 2016). As for the

reaming 4 transmembrane segments, S1-S4, they form a module that somehow controls the opening and closing of the pore. Particularly, S4 contains lysine or arginine appears in every third or fourth position in an otherwise hydrophobic stretch and is thought to form the voltage-sensing element of Kv channels.



1.1.3 A-type potassium channels

Of ~350 ion channel types expressed in the mammalian brain, including 145 voltage-gated channels, there are 40 of them are voltage-gated potassium (Kv) channels and the superfamily is divided into 12 sub-families (Kv1 – Kv12) based on their amino acid sequence homology (Ranjan et al., 2019). Among them, KCNA4 (Kv1.4) and KCND family, including Kv4.1, Kv4.2 and Kv4.3, constitute the A-type K⁺ channel that mediate A-type K current (I_A). Compared to the other members, Kv4.2 and Kv4.3 are predominant in the brain (Birnbaum et al., 2004; Carrasquillo et al., 2012). In addition to voltage-gated, A-type K⁺ channels also have features of low threshold (usually lower than that of action potential (AP)) for activation, fast activation, and rapid inactivation with a time constant typically 15-50 ms (Storm, 1990). In fact, these features result in I_A with a waveform similar to an English alphabet A, after which the current is named. A-type Kv channels serve numerous functions in neuron, including the regulation of excitability, fast-spiking, neurotransmitter release in neural networks during physiological and pathophysiological processes. In hippocampal neurons, I_A is reported to participate in the regulation of dendritic calcium signaling, synaptic integration, and synaptic plasticity (Chen et al., 2006). In the noradrenergic neurons of the A7 catecholamine cell groups in the pons, the brainstem I_A plays important roles in shaping AP waveform, tuning AP firing frequency, and synaptic integration (Min et al., 2010). In mice with “necdin” deficiency, an animal model of Prader-Willi syndrome, there is an



abnormal high AP frequency of the noradrenergic neurons of the locus coeruleus (LC) due to the upregulation of I_A (Wu et al., 2020). Interestingly, a common feature of Prader-Willi syndrome is that the individual shows attention deficiency and high LC neuron firing rate is well known to lead to distraction and anxiety.

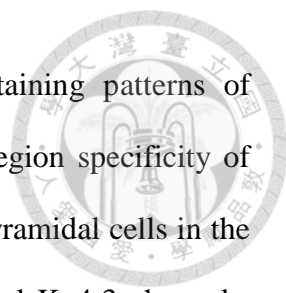
1.2 Kv4.2

1.2.1 Overview

The Kv4.2 channel subfamily D member 2 (KCND2) is a member of shal-related subfamily (KV4 family) encoding the pore formation alpha subunits of Kv channels mediating I_A (KCND2 from ncbi, GeneID: 16508, 2021). In addition to the alpha subunits, Kv4.2 channels may be also associated with 2 classes of auxiliary subunits: dipeptidyl-peptidase-like type II transmembrane proteins typified by DPPX-S and cytoplasmic Ca^{2+} binding proteins known as K^+ channel interacting proteins (KChIPs). The auxiliary subunits play distinct roles in modulating the biophysical properties of Kv4.2; they have different structures and binding sites on Kv4.2 and exert similar effects on Kv4.2 trafficking but distinct effects on Kv4.2 gating. (Seikel, and Trimmer, 2009)

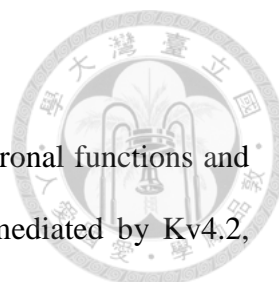
1.2.2 Distribution of Kv4.2

Kv4.2 subfamily has a widespread distribution throughout the mouse brain; especially, the channels are prominently presented in striatum, hippocampus and cerebellar cortex (Clark, et al., 2008). They mediate I_A to set AP threshold, waveform, and firing frequency in the neurons of these brain regions (Alfaro-Ruiz et al., 2019). For example, there is a high density of immunoreactivity (ir) for Kv4.2 and the auxiliary subunits, KChIPs 2, 3, and 4 in the in hippocampus CA1 and dentate gyrus.



Interestingly, the signals have a close correspondence in the staining patterns of antibodies against Kv4.3. Moreover, there are also cell-type and region specificity of kv4.2-ir signal and the close correspondence Kv4.3-ir signal. The pyramidal cells in the CA3 and granule cells in the dentate gyrus express both Kv4.2 and Kv4.3 channels, while CA1 pyramidal cells only express Kv4.2. In the CA1 to CA3, Kv4.2-ir is concentrated in the stratum oriens (so) and stratum radiatum (sr), which contain, respectively, the basal and apical dendritic arbors of pyramidal cells. Furthermore, the Kv4.2-ir signal in the CA1 stratum radiatum is not uniform, but drops significantly in the distal portion of the dendrite (Rhodes et al., 2004). At subcellular level, Kv4.2-ir signals are found at dendritic spines of principal cells and are proximity to postsynaptic densities (PSDs), indicating that the Kv4.2 functionalities could be modulated by synaptic activity.

In the cerebellar cortex Kv4.2-ir and DPP6-ir signals are observed predominantly in the granule cell layer, but neither in of Purkinje cells or the interneurons in the molecular layer. At subcellular level, both Kv4.2 and DPP6 proteins are enriched in the granule cell dendrites, producing a strong stained structure so called, cerebellar glomeruli, where the dendrites of the granule cells contact unstained cerebellar mossy fiber axons. The density of Kv4.2-ir and Kv4.3-ir signals increases significantly from the soma towards dendritic spines, demonstrating an uneven distribution of the two channel subtypes along the neuronal surface of granule cells. The similar somato-dendritic gradient found for Kv4.2 and Kv4.3 along neuronal surface of the granule cells favors the idea that they are likely to form heterotetrameric Kv4.2/Kv4.3 channels in the granule cells.



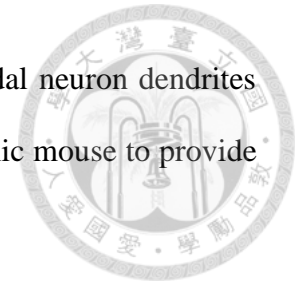
1.2.3 Functional role of Kv4.2

Previous studies have revealed important roles of Kv4.2 in neuronal functions and behavior. In hippocampal CA1 neurons, I_A conductance, mainly mediated by Kv4.2, contributes action potential back propagation along dendrites and the dendritic computation (Migliore et al., 2005; Chen et al., 2006). A reduced Kv4.2 due to rapid internalization of the proteins upon the glutamate receptor activation can lead to an enhancement of miniature excitatory postsynaptic currents (mEPSC) amplitude (Kim et al., 2007). On the other hand, activation of NMDA receptor can enhance Kv4.2 translation via inhibition of fragile X mental retardation protein (FMRP) that serves as a means for negative feedback regulation for synaptic homeostasis (Lee et al., 2011). These studies indicate a role of Kv4.2 in activity-dependent regulation on dendritic computation. Kv4.2 also plays an important role in development. In retina, Kv4.2-mediated currents are important for postnatal development in a subset of retinal ganglion cells (RGCs) (Qu et al., 2009). In human Kv4.2 impairment is reported to be associated with early-onset global developmental delay (Zhang et al., 2021).

1.2.4 Transgenic mice in Kv4.2 research

To further explore the functional role of Kv4.2, transgenic tools that can provide a lost/gain function by manipulating Kv4.2 expression are essential. For example, by using Kv4.2 KO transgenic mice, an increase in excitability in the dorsal horn neurons receiving nociceptive information due to the attenuated I_A -type current has indicated the role of Kv4.2 in regulating transmission of nociceptive signals (Hu et al., 2006). In addition, Kv4.2 KO mice also show a phenotype of abnormal serotonin release that leads to an elevated immobility in forced swimming test (Lockridge et al., 2010). At subcellular level, Kv4.2 KO increased fraction of NR2B/NR2A, two NMDA receptor

subunits, and enhanced LTP via calcium signaling in CA1 pyramidal neuron dendrites (Jung et al., 2008). These works indicate the value of using transgenic mouse to provide us innumerable knowledge about Kv4.2 functions.



1.2.5 The need of site specific KO in adult mouse in Kv4.2 research

A potential weakness of systemic KO mice has been the associated unwanted side effects that could interfere with the data interpretation. For example, using conventional pharmacological approach to inhibit Kv4.2 function in specific brain regions have revealed provided results different from those of studies using *Kv4.2* KO mice. It has been shown that *Kv4.2* KO mice exhibited spatial learning impairment in Morris Water Maze test (Hu et al., 2020). On contrast, reducing Kv4.2 activity by infusion of a specific Kv4.2/Kv4.3 channel blocker, PaTx, into CA3 somatic area to repress afterhyperpolarization in aged rats restored intrinsic excitability property of the aged CA3 pyramidal neurons to a young-like state (Simkin et al, 2015). Accordingly, it is actually suggested that inhibition of Kv4.2 function in aged animals may prevent and/or ameliorate the aging-related cognitive deficit but not impairs memory (Oh et al., 2016). The discrepancy could be ascribed to aged issue and/or the use of difference approach, namely, region-specific inhibition of Kv4.2 function *versus* systemically *Kv4.2* KO. Moreover, *Kv4.2* KO mice exhibit dramatic decreases in the cellular and subcellular expression of specific KChIPs that reflected their degree of association and colocalization with Kv4.2 in wild-type mouse and rat brains (Menegola et al., 2012). Impairment of Kv4.2 function in transgenic mice may undergo abnormal development. Thus, the assumed functional role of Kv4.2 may partially be developmental effect.

To have better understanding of the functional roles of Kv4.2 in specific behaviors

and brain functions, re-examination of functional read out upon tissue-specific *Kv4.2* KO in adult is necessary.



1.3 Aim of this study

To explore the role of *Kv4.2* in specific brain areas, I followed the approach described in the Master thesis work of the Department of Life Science at NTU by Miss Chen. In the work, an adeno-associated virus (AAV) that can conduct site specific *Kv4.2* knockout (KO) was designed using CRISPR/ Cas9 system (Chen, 2019). The system has been proved effective by morphological IHC methods.

Here I wish to further prove functional evidence for its effectiveness using whole-cell variant of patch clamp recording from CA1 pyramidal cells in hippocampal slices. The pyramidal cells are targeted because the cells are well known to exhibit A-type potassium current (I_K) mediated by *Kv4.2* and the channel's functional role is well characterized (Chen et al., 2006).

Chapter 2. Materials and Methods

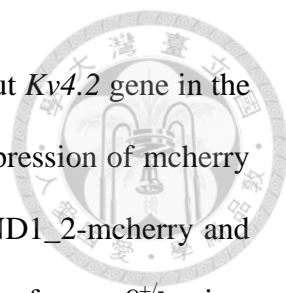


2.1 Animals

B6J129(B6N)-Gt(ROSA)26Sortm1(CAG-cas9*,-EGFP)Fezh/J mice (*cas9* mice) (Platt et al., 2014) purchased from the Jackson Lab (stock #026175; Bar Harbor ME, USA) were used. These mice have cre-recombinase-dependent expression of CRISPR associated protein 9 (*cas9*) endonuclease and EGFP directed by a CAG promoter. Littermate genotypes were confirmed by PCR results on the basis of cre-specific primers (forward, ACA CCA GCA CCA AAG AGG TG; reverse, GTA GGT CAG GGT GGT CAC CA) and neo-specific primers (forward, AAG GGA GCT GCA GTG GAG TA; reverse, CCG AAA ATC TGT GGG AAG TC). Only heterogeneous mice were used for all experiments. In a series of experiments, offspring of *cas9* mice crossed with *CamKII α -iCre* mice (from Dr. C.-K. James Shen at Academia Sinica, Taiwan) were used. The heterozygous offspring (*cas9*^{CamKII α -iCre} mice) expressed floxed *cas9* allele and *cre* transgene. As ^{CamKII α -I} are predominantly express in principal neurons including the cortical and hippocampal pyramidal cells (Casanova et al., 2001), *cas9*^{CamKII α -iCre} mice would have CRISPR/ Cas9 system in their cortical and hippocampus pyramidal cells without additional application of cre. Littermate genotypes were confirmed by PCR results on the basis of *CamKII α* -specific primers (forward, CTC TGA CAG ATG CCA GGA CA; reverse, TGA TTT CAG GGA TGG ACA CA)

2.2 Virus

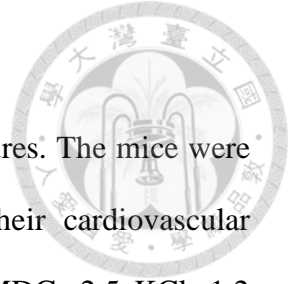
AAV9-SpKCND1_2-mcherry (titers: 9.77×10^{12} vg/mol) and AAV9-CMV-cre (titers: 8.43×10^{12} vg/mol) will be used for Kv4.2 knockout. The AAV9-CMV-cre provides cre-recombinase for triggering *cas9* and EGFP expression. The EGFP are used as indicator of cre expression in CA1 neurons. The AAV9-SpKCND1_2-mcherry



provides sgRNA which guides CRISPR/Cas9 to specifically knockout *Kv4.2* gene in the CA1 pyramidal cells expressing cre/EGFP; the virus also allows expression of mcherry as an indicator for sgRNA expression. A mixture of AAV9- SpKCND1_2-mcherry and AAV9-CMV-cre(2:1) was used for injection into the hippocampus for *cas9*^{+/-} mice; while AAV9- SpKCND1_2-mcherry alone was used for *cas9*^{CamKII α -iCre} mice. AAV9-PX552-mcherry (titers: 8.66×10^{11} vg/mol), which contains plasmid backbone of AAV9-SpKCND1_2-mcherry without sgRNA insertion, was used as control virus.

2.3 Stereotaxic surgery

Viruses were injected into the dorsal hippocampi of mice aged 4-7 weeks using the following standard procedures. The mice were anesthetized by a mixture of anesthetics containing zoletil (50mg/kg) and xylazine (5mg/kg) via intraperitoneal injection. The mice were then mounted on a stereotaxic apparatus. After positioning and drilling through the braincase, two infusions of AAV(s) were made with into the CA1 region of the hippocampus using following coordinate: -2.8 mm anteroposterior (AP); ± 2.7 mm mediolateral (ML) ; -1.1 mm dorsoventral (DV), and -3.3 mm AP; ± 3 mm ML; -1.5 mm DV. Unless specified otherwise, the infusions were made bilaterally and 100 nL AAV(s) for each were delivered. The infusions were made with a glass pipette mounted to a 2.0 μ L Hamilton microsyringe (Neuros Model 7002 KH, Hamilton, Reno, NV, USA). The pipette was beveled using a microelectrode beveler (BV-10, Sutter Instrument, Novato CA, USA) and its tip had an opening diameter of 20-50 μ m. The AAV(s) was slowly infused at a speed of 20 nL/min⁻¹. The animals were allowed to recover for 4-7 weeks after surgery before the commence of the physiological recording.

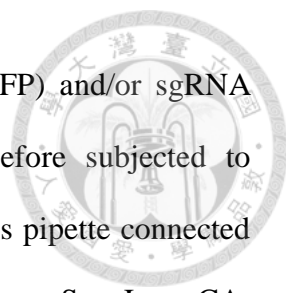


2.4 Preparation of hippocampal slices

Hippocampal slices were prepared using the following procedures. The mice were anesthetized by lethal dose of urethane and perfused through their cardiovascular system with ice-cold cutting solution containing (in mM): 93 NMDG, 2.5 KCl, 1.2 NaH₂PO₄, 30 NaHCO₃, 20 HEPES, 25 Glucose, 10 MgSO₄, 0.5 CaCl₂, 5 sodium ascorbate, and 3 sodium pyruvate; the osmolality adjusted to 310 mOsm with glucose and the pH to 7.35. The solution was saturated with 95% O₂/5% CO₂. The hippocampi from the both hemispheres were quickly cut out and sliced at a thickness of 300 μm using with a vibratome (Leica VT1000S, Leica Biosystems, Nussloch, Germany). The slices were incubated with the cutting solution in a holding chamber at room temperature for 15 minutes, followed by incubation at 37°C for 15 minutes. The slices were incubated with regular artificial cerebrospinal fluid (ACSF) for at room temperature for at least 60 minutes before moving to the recording chamber. The ACSF contained (in mM): 92 NaCl, 2.5 KCl, 1.2 NaH₂PO₄, 30 NaHCO₃, 20 HEPES, 25 glucose, 2 MgSO₄, 2 CaCl₂, 5 sodium ascorbate, and sodium pyruvate; the osmolality adjusted to 305 mOsm with glucose and the pH to 7.35. The solution was saturated with 95% O₂/5% CO₂.

2.5 Whole-cell clamp recording

The recording chamber was mounted to an upright microscope (BX51WI, Olympus Optical Co., Ltd, Tokyo, Japan) equipped with 40× water immersion objective, Nomarski and epifluorescence optic systems and an ORCA-R2 camera (Hamamatsu Photonics, Shizuoka, Japan). For whole cell variant of patch-recording was made from pyramidal cells in CA1 region under visual guidance with the Nomarski optic system. Neurons with a triangular cell body in the stratum pyramidale and apical dendrite in the



stratum radiatum were targeted. They were validated for cas9 (GFP) and/or sgRNA (mCherry) expression using the epifluorescence optic system before subjected to whole-cell recording. The electrical signal was recorded with a glass pipette connected to the headstage of a Multiclamp 700B amplifier (Molecular Devices, San Jose, CA, USA). The pipette was pulled from a borosilicate glass capillary (GC150F-10, Warner Instruments, Hamden, CT, USA) and had a resistance of 7–10 MΩ when filled with intracellular solution containing (in mM): 2 EGTA, 131 K-Gluconate, 10 HEPES, 2 KCl, 8 NaCl, 2 ATP, and 0.3 GTP, the pH adjusted with KOH and osmolarity to 300 mOsm with sucrose. Biocytin of 12.5 mg/ml was routinely included in the intracellular solution to fill the recorded neurons for *post hoc* validation of their morphology. To isolate voltage evoked potassium currents, the recording was performed in condition in which 1mM TTX was added and Ca²⁺ was omitted in the ACSF to block Na⁺ currents, Ca²⁺ currents/ Ca²⁺-activated potassium currents, respectively. The signals were low-pass filtered at a corner frequency of 2 kHz and digitized at 10 kHz using a Micro 1401 interface running Signal software (Cambridge Electronic Design, Cambridge, UK). Capacitive currents will be compensated digitally by using null traces or scaled traces of smaller voltage steps. Serial resistance was compensated by at least 70% and monitored by applying a 5 mV test pulse in each frame. Leak currents were subtracted using function provided by the Signal software.

To measure *reversal potential* (E_r) of the voltage evoked potassium current (I_K), V_m was first stepped from -100 to 0 mV (duration: 5 ms), followed to a level ranging from -20 to -120 mV with 10 mV increments. The peak of the evoked peak tail currents were measured and plotted against the membrane voltage. The constructed I–V relationship was fitted with a quadratic polynomial (Bekkers, 2000), and the membrane voltage when whole-cell current equaled 0 as taken as E_r .

To measure *voltage-dependent activation*, a similar paradigm described above was employed, except that the voltage pulse was gradually stepped from -100 mV to +65 mV in 15 mV increments. The conductance of the I_K was calculated as:

$$G(V)=I(V)/(V-E_r),$$

where $G(V)$ is the conductance of the I_T with the V_m commanded to V , E_r is the I_K reversal potential described above (Fig. 2), and $I(V)$ the I_K peak amplitude with the V_m commanded to V . The activation curve was constructed by plotting V against $G(V)$ and was fitted to a fourth-order Boltzmann equation:

$$G(V)=A_0/(1+\exp(-(V-V_{1/2})/k))^4,$$

where V is the membrane potential, $V_{1/2}$ is the membrane voltage at which half of the maximum conductance is achieved, k the slope factor, and A_0 a constant (Min et al., 2010).

To measure *voltage-dependent inactivation of I_K* , a voltage pre-pulse was first stepped to various levels (-100 mV to -0 mV in 10 mV increments) and then to 50 mV. The peak amplitudes of the I_K evoked by the 50 mV pulse with different pre-pulse levels were measured and normalized to the largest amplitude. The inactivation curve was constructed by plotting V against the normalized peak amplitude of the I_K and was fitted to the Boltzmann equation:

$$I(V)=A_0/(1+\exp((V-V_{1/2})/k)),$$

where V is the membrane potential, $V_{1/2}$ the potential at which half of the peak I_K amplitude is achieved, k the slope factor, and A_0 a constant.

To measure the *time-dependent recovery from inactivation*, two conditioning pulses with a duration of 0.8 s and stepped from -100 mV to -10 mV were applied. The inter-pulse interval was varied from 10 to 200 ms in increments of 10 ms. The recovery curve was constructed by plotting the inter-pulse interval against the peak amplitude of the I_K

evoked by the first pulse divided by the peak amplitude of the I_K evoked by the second pulse and was fitted to a single exponential function:

$$I(t)=A_0+A_1/(1-\exp(-t/\tau)),$$

where $I(t)$ is the peak current ratio at the inter-pulse interval t and A_0, A_1 are constants.



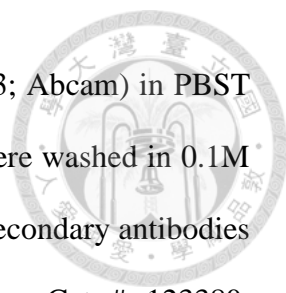
2.6 Immunohistochemistry

2.6.1 Perfusion

Mice were first perfused through the cardiovascular system with 20 ml saline (0.9% NaCl), followed with perfusion of 50 ml 4% paraformaldehyde (PFA) in 0.1M phosphate buffer (PB). The brains were carefully dissected out and then immersed in the PFA for post-fixation for at least 4 hours. After the post-fixation, the brains were transferred to 30% sucrose solution in 0.1M PB in 4°C overnight for cryoprotection. The brains were cut into consecutive coronal sections of 50 μ m thickness using frozen sectioning method. The sections were subjected to the following immunohistochemistry. The sections prevented from light to avoid fluorescence decay during the IHC staining procedures.

2.6.2 IHC for Kv4.2

Sections comprising the AAV transfection were collected for IHC using antibodies against Kv4.2. The sections were first washed in 0.1M PB for 3 times, each for 5 minutes, followed by wash with PBST (0.01M PB, 0.09 NaCl, 0.1% TritonX100) for 10 minutes. The sections were then incubated with 2% bovine serum albumin (BSA) (Jackson ImmunoResearch Laboratories, Cat. #: 001-000-62; West Grove, PA, USA) and 10% normal goat serum (NGS) (Cat. #: ab7481; Abcam, Cambridge, UK) in PBST buffer for 1.5 hrs to block nonspecific reactions. The sections were then incubated with



primary antibodies against Kv4.2 (1:1000 dilution; Cat. #: ab123543; Abcam) in PBST at 4°C overnight. After primary antibody incubation, the sections were washed in 0.1M PB for 3 times, each for 5 minutes. They were then incubated with secondary antibodies of DyLight 405- conjugated Goat anti-rabbit antibody (1:200 dilution; Cat. #: 123380; Jackson ImmunoResearch Laboratories) in PBST at room temperature on for 2 hours. After 3 times of X-minute wash with 0.1M PB, the sections were air-dried on microscope slides and coverslipped with Rapid Clear Mounting Medium (Cat. #: RCCS002; SUNJin Lab, Hsinchu, Taiwan). The sections were continuously shaken on a shaker during the entire staining procedures.

2.6.3 *Post hoc* biocytin histochemistry

The brain slices were immersed in 4% PFA for fixation after electrophysiological recording. They were then subjected to biocytin histochemistry for revealing the morphology without further sectioning. The slices were washed 3 times, 5 minutes for each, with 0.1M PB and then incubated with 2% BSA in PBST buffer for 1.5 hours. The slices were then incubated with DyLight 405-conjugate streptavidin (1:100 dilution; Cat. #: 133643, Jackson ImmunoResearch Laboratories) for 2 hours. After the incubation, the slices were washed with 0.1M PB 3 times, each for 5 minutes, and soaked in Rapid Clear Mounting Medium for 1 hour. Subsequently, the slices were mounted on slides and cover slipped with the same mounting medium.

2.7 Confocal imaging

The slices and sections were examined with a Zeiss LSM 780 confocal microscope. Figure adjustments were processed in Zen black edition.

Chapter 3. Results

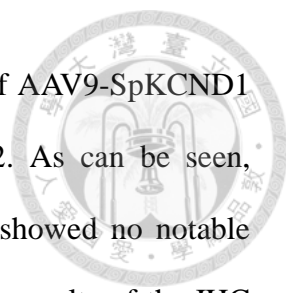
3.1 IHC examination of Kv4.2 KO with CRISPR/Cas9 method in adult

hippocampus

To have a quick examination the effectiveness of the CRISPR/Cas9 method, I first employed IHC to investigate the protein expression level of Kv4.2. In this series of experiments, *cas9* and *cas9*^{CamKII α -iCre} mice were used; *cas9* mice received a mixture of AAV9-SpKCND1_2-mcherry (for sgRNA delivery) and AAV9-CMV-cre infusion (cre delivery) with a ratio of 2:1 (*sgRNA* vs. *cre*) and *cas9*^{CamKII α -iCre} mice received AAV9-SpKCND1_2-mcherry infusion only. The AAV infusion was made to one side of the hippocampus and the contralateral side was used as the IHC control. The IHC of Kv4.2 was conducted 4 weeks after the AAV infusion. A typical example of the results using *cas9*^{CamKII α -iCre} mice is shown in Fig. 1. Consistent with previous reports (Alfaro-Ruiz et al., 2019), CamKII α -iCre (GFP) expression was found predominantly in principal neurons (see green in Fig. 1A1, A2, B1, B2, C1, C2, D1 & D2). In the control side (Fig. 1 C4, D4), the signal of Kv4.2 immunoreactivity (ir) was observed all over the entire hippocampus, with an exception that the Kv4.2-ir signal was very weak in the stratum pyramidale of the CA1 and CA3 regions and in the granule cell layer of the dentate gyrus. In the AAV injection side, the sgRNA expression covered a part of CA1 region as well as a part of dorsal molecular and granule cell layers of the dentate gyrus (Fig. 1A3, B3). Notably, the Kv4.2-ir signal in these region was significantly reduced (see asterisk in Fig. A4, B4). Similar observations were repeated in additional 3 *cas9*^{CamKII α -iCre} mice and in 2 *cas9* mice.

To exclude the possibility that the above observations were due to plasmid delivery, regardless of the existence of correct sgRNA, I also performed AAV control experiment in which all experimental procedures were repeated with an exception that the control

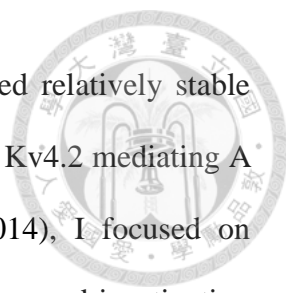




virus (AAV9-PX552-mcherry) for empty plasmid delivery instead of AAV9-SpKCND1 was used; a typical example of the results is shown in Figure 2. As can be seen, compared to the control side (Fig. 2C4, D4), the Kv4.2-ir signal showed no notable reduction in the AAV infusion side (Fig. 2C3, D4). In summary, the results of the IHC study show that the AAV9-SpKCND1 is effective and could be useful for performing CRISPR KO of Kv4.2 channel in a cell-type specific manner in adult brain.

3.2 A-type potassium current characterization


To confirm the results of the IHC study, I also employed electrophysiological method to examine the effectiveness of the AAV9-SpKCND1. To this end, I made whole-cell variant of patch-clamp recording from CA1 pyramidal cells and compared between the voltage-dependent I_K recorded from control cells (no cre and sgRNA expression or expressed the either gene only) and the cells expressing cre and sgRNA. Before the CRISPER manipulation of Kv4.2 expressions, I first validated the consistency of the properties of fast activating I_K in my study compared to the previous studies. In this series of experiments, 5 *cas9* and 3 *cas9*^{CamKII α -iCre} mice were used, and the mice received no AAV infusion. The E_r of the I_K was measured by recording tail current of fast activating K^+ channels at various membrane voltage (see arrow in Fig. 3A & B), and a value of -66.92 mV was obtained in my recording condition (see Materials and Methods). This value was highly compatible to the value, -65 mV, reported by a previous study conducted in A7 catecholamine neurons (Min et al, 2010). This could be due to the fact that my recording conditions, especially, the ionic composition of intra-/extracellular solutions, are very similar to this study. In responding to voltage step from -70 mV to 65 mV, an outward I_K was evoked (Fig. 4A). The I_K had a transient component (I_{K-T}) displaying rapidly activated and inactivated (see



asterisk in Fig. 4A) and a sustained component (I_{K-S}) that remained relatively stable during the ending phase of stimulation (see arrow in Fig. 4A). Since Kv4.2 mediating A-type I_K features rapid activation and inactivation (Liu et al., 2014), I focused on analyzing the dynamics of the I_{K-T} . Both voltage-dependent activation and inactivation curves of I_{K-T} were constructed and fitted with Boltzman equation (Fig. 4A-C). The voltage-dependent activation curve revealed that I_{K-T} has low activation threshold (~ 55 mV) and half-activation voltage ($V_{1/2} = 0$ mV) and a fast activation dynamic ($k = 12$) value; the voltage-dependent inactivation curve revealed features of fast inactivation (half inactivation voltage, $V_{1/2} = -41$ mV and $k = -12$) (Fig. 4C). The two curves overlap over a membrane voltage range from -55 to 15 mV, indicating that I_{K-T} could be operating at subthreshold membrane voltage. The I_{K-T} recovered from inactivation quickly with time constant (τ) of 75.9 ± 43.4 ms (Fig. 3C, 3D). In summary, the reported dynamic characteristics of the I_{K-T} in my study are consistent with the Kv4 mediating I_{K-T} reported in A7 catecholamine neurons (Min et al., 2010) and hippocampal CA1 pyramidal neurons (Hoffman et al., 1997). Accordingly, the I_{K-T} recorded at soma in my study might involve the current mediated by Kv4.2, though the subcellular distribution of the proteins was reported to be at the dendrites, which is also confirmed in my IHC study (Figures 1 & 2).

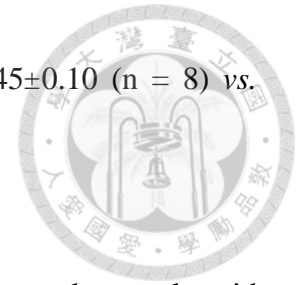
3.3 Kv4.2 KO in hippocampal CA1 pyramidal neurons leads to decreased A-type potassium currents.

I next examined the effectiveness of the AAV9-SpKCND1 by comparing I_{K-T} between control cells and pyramidal cells with Kv4.2 KO. In this series of experiments, 7 *cas9* and 16 *cas9*^{CamKII α -iCre} mice were used, and they were sacrificed for brain slice preparation and electrophysiological recording 4 weeks after AAV(s) infusion. Hereafter,



I referred cells expressing cre/GFP and sgRNA/mcherry to Kv4.2-KO and cells expressing none or one of the either gene to control cells. These expression profiles were quickly validated online before whole-cell recording and were further confirmed by *post hoc* histochemistry (Figs. 5, 6). The membrane potential was clamped at -70 mV, and I_K was evoked by gradual voltage steps to 65 mV with increment of 15 mV (Fig. 7A1, 7B1, 7C1). For comparison of I_K among pyramidal cells, the peak I_{K-T} amplitude recorded from an individual cell was normalized to the cell's soma area, measured from online Normaski image, to yield current density. I found no significant difference in I_{K-T} density between control and Kv4.2-KO cells (CTRL vs. KO: 8.64 ± 4.35 (n = 18) vs. 7.58 ± 3.23 (n = 11) nA/mm², p = 0.245, *t*-test) (Fig. 8A). However, I_{K-S} appeared to be larger and the I_{K-T} decay rate appeared to be slower in Kv4.2-KO cells than in control cells (Fig. 7A, B). Accordingly, I also statistically compared I_{K-S} density between Kv4.2-KO and control cells, and found that there might be a potential difference (CTRL vs. KO: 2.61 ± 0.97 (n= 18) vs. 3.19 ± 1.23 (n=11) nA/mm², p=0.083 *t*-test) (Fig. 8B). By comparing the ratio of I_{K-T} density to that of I_{K-S} , the parameter did exhibit a significant difference between Kv4.2-KO and control cells (CTRL vs. KO: 3.28 ± 0.69 (n=19) vs. 2.37 ± 0.50 (n=11), p=0.0003 *t*-test) (Fig. 8C). These results raise a possibility that KO of Kv4.2 mediating A-type I_K might be associated with an up-regulated I_{K-S} to compensate the I_K . To directly test this possibility, I compared 4-AP, a broad spectrum A-type I_K blocker, sensitive current recorded in Kv4.2-KO and control cells. Bath application of 10 mM 4-AP dramatically reduced the peak I_{K-T} amplitude, but did not affect the I_{K-S} . The 4-AP sensitive current density was obtained by subtraction of I_K recorded during from that before 4-AP application; the subtracted current was again normalized to cell body area to yield current density, then normalized to the peak I_{K-T} amplitude. As can be seen, normalized 4-AP sensitive current density in Kv4.2-KO cells was significantly

reduced compared to that of the control cells (CTRL vs. KO: 0.45 ± 0.10 (n = 8) vs. 0.32 ± 0.08 (n = 7) nA/mm², p=0.0094 *t*-test) (Fig. 7, Fig. 8D).



Again, to exclude the possibility that the above observations were due to plasmid delivery, I further performed AAV control experiment in which all recording procedures were repeated with an exception that the control virus (AAV9-PX552-mcherry) for empty plasmid delivery instead of AAV9-SpKCND1 was used. Cells expressing cre/GFP and PX522/mcherry were target for whole-cell recording and referred to virus control (CTRL virus) cells. Consistently, no significant difference in I_{K-T} density was observed between Kv4.2 KO and CTRL virus cells (KO vs. CTRL virus: 7.58 ± 3.23 (n=11) vs. 6.72 ± 2.59 (n = 9) nA/mm², p = 0.263, *t*-test) (Figure 7, Fig. 8A), and significant difference was observed in I_{K-S} density (KO vs. CTRL virus: 3.19 ± 1.23 (n = 11) vs. 2.36 ± 0.51 (n=9) nA/mm², p = 0.0376 *t*-test) (Figure 7, Fig. 8B), ratio of I_{K-T} density to that of I_{K-S} (KO vs. CTRL virus: 2.37 ± 0.50 (n = 11) vs. 2.81 ± 0.59 (n = 9), p = 0.044 *t*-test)(Figure 7, Fig. 8C), and 4-AP sensitive current density (KO vs. CTRL virus: 0.32 ± 0.08 (n = 7) vs. 0.39 ± 0.06 (n = 8) nA/mm², p = 0.0478 *t*-test) between the two groups.

Chapter 4. Discussion

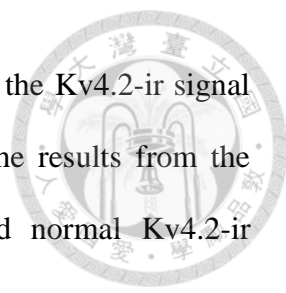


4.1 Overview

In this study, effectiveness of the AAV9-SpKCND1 is tested by both IHC and electrophysiology. The AAV delivers sgRNA that is designed to guide Cas9 to delete Kv4.2 genes in the target neurons, and my results provide strong evidences showing that the AAV is indeed very effective. This proof-of-concept study convinces that, with powerful platform for precise sgRNA design, ion channels, receptors and neurotransmitter synthesis etc., can be effectively knocked out in the central nervous neurons of adult mouse in region-specific and cell-specific manners by combining Cre-Lox system, CRISPR/Cas9 system, and viral transfection methods. This certainly a powerful tool for examination of the functional role of a particular protein in processing information in the neuronal network and the mechanism underlying brain diseases related to the protein malfunction.

4.2 Effect of site-specific Kv4.2 KO in adult on Kv4.2 expression pattern

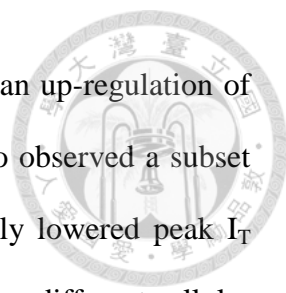
My IHC results show that the Kv4.2-ir was significantly decreased in regions expressing both cre-recombinase and the sgRNA. These results are consistent with Chen's studies (Chen, 2020), and show that the AAV9-SpKCND1 can effectively guide Cas9 expressed in the target pyramidal cells to conduct gene edition in adult mice. The accuracy of the IHC results critically depends on specificity of the Kv4.2 antibody. Based on the following facts, I am confident that my IHC results is reliable. First, the Kv4.2-ir signal (see Figs. 1 and 2) pattern in the hippocampus is consistent with previous report (Alfaro-Ruiz et al., 2019). Second, only regions where the cre and sgRNA expression overlap, there is a reduction of the Kv4.2-ir signal, compared to contralateral control hippocampus. In addition, for those region where there is no



overlap of the cre and sgRNA expression in the AAV injection site, the Kv4.2-ir signal show no difference, compared to the contralateral control side. The results from the experiments using control AAV (AAV9-PX552-mcherry) showed normal Kv4.2-ir signal further support the reliability of my IHC results.

4.3 Effect of site-specific Kv4.2 KO in adult on A-type potassium current

In my electrophysiological study, an interesting observation is that, the Kv4.2-KO cells showed no significant difference in I_{K-T} but a significant decrease in the ratio of I_{K-T} to I_{K-S} , compared to control cells and CTRL virus group. Previous studies using Kv4.2 KO transgenic mice reported a significant change, compared to wild-type mice, a significant change in I_T but not I_S in the spinal cord dorsal horn neurons (Hu et al., 2006), left ventricular aneurysm (LVA), interventricular septum myocytes (Guo et al., 2005), and hippocampal neurons (Chen et al., 2006). My observation showing a significant reduction of 4-AP sensitive current density in Kv4.2-KO cells is consistent with these studies. In addition, my observation of a significant difference in the I_{K-T} to I_{K-S} would suggest a compensated upregulation of other Kv channels. However, Chen et al (2006) also reported that synaptic proteins, Kv4.3, Kv3.4, and Kv1.4, among other channels, are not significantly altered in the hippocampus of Kv4.2 knockout mice. Furthermore, their IHC study showed unaltered expression level or subcellular distribution of Kv4.3, but a dramatic decrease in cellular and subcellular expression of specific KChIPs that are closely associated with Kv4.2 in hippocampus. It is accordingly possible that, similar to KChIPs enhancing Kv4.2 function, auxiliary proteins that could enhance I_{K-S} are upregulated in Kv4.2-KO cells in my study. Interestingly, Nerbonne et al. (2008) reported no significant difference in I_{K-T} but a significant decrease in I_{K-S} and I_{K-T} to I_{K-S} in the pyramidal cells in the visual cortex.



These observations exactly match the results of my study; namely, an up-regulation of delayed rectifier Kv current components, the I_{K-S} . Meanwhile, I also observed a subset of Kv4.2-KO cells showed similar I_{K-T} to I_{K-S} ratio but significantly lowered peak I_T amplitude. These studies suggested that deletion of Kv4.2 could trigger different cellular response in different pyramidal cells.

4.4 Methodology Considerations

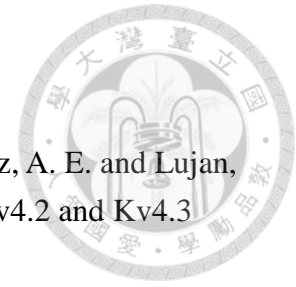
CTRL virus infection showed no difference in Kv4.2-ir compared to non-infected side. However, CTRL virus group showed significant decrease in I_{K-T} to I_{K-S} ratio compared to CTRL group. One possible explanation is that stereotaxic surgery caused some effect to A-type I_K so that the ratio was decreased, while normalized 4-AP sensitive current was not significantly changed. Although virus infection may influence A-type I_K , Kv4.2 cell KO group and CTRL virus group, both received virus infection, showed significant difference in I_{K-T} to I_{K-S} ratio and normalized 4-AP sensitive current. As a consequence, the effectiveness of Kv4.2 KO virus can still be proved by these electrophysiology experiments.

Another methodological consideration is that in *post hoc* examination of virus infection using biocytin histochemistry, significant decrease in the contrast of both GFP and mcherry signals is observed under confocal microscope, compared to the on-line Normazki (IR-DIC) images. One possible reason is that electrophysiological recording caused cell context loss and cell swelling. Fluorescent molecules outflowed or were dispersed into a lower concentration, leading to a lowered fluorescent signal. As a consequence, identification of KO group and CTRL virus group is solely done by IR-DIC photo. The *post hoc* images can only provide cell type information and

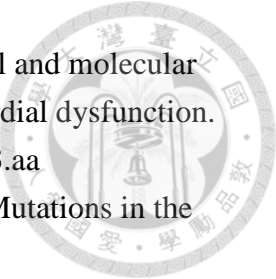
supporting evidence of virus infection.



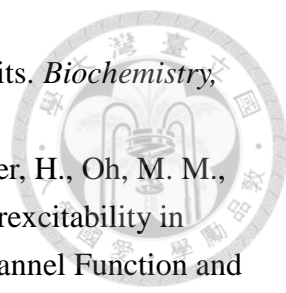
Chapter 5. Reference



- Alfaro-Ruiz, R., Aguado, C., Martin-Belmonte, A., Moreno-Martinez, A. E. and Lujan, R. (2019). Expression, Cellular and Subcellular Localisation of Kv4.2 and Kv4.3 Channels in the Rodent Hippocampus. *Int J Mol Sci*, 20(2).
doi:10.3390/ijms20020246
- Bekkers, J. M. (2000). Properties of voltage-gated potassium currents in nucleated patches from large layer 5 cortical pyramidal neurons of the rat. *J Physiol*, 525(Pt 3):593-609. Doi:10.1111/j.1469-7793.2000.t01-1-00593.x
- Birnbaum, S. G., Varga, A. W., Yuan, L. L., Anderson, A. E., Sweatt, J. D., and Schrader, L. A. (2004). Structure and function of Kv4-family transient potassium channels. *Physiol Rev*, 84:803–833. doi:10.1152/physrev.00039.2003
- Carrasquillo, Y., Burkhalter, A., and Nerbonne, J. M. (2012). A-type K⁺ channels encoded by Kv4.2, Kv4.3 and Kv1.4 differentially regulate intrinsic excitability of cortical pyramidal neurons. *J Physiol*, 590(16):3877-90.
Doi:10.1113/jphysiol.2012.229013
- Casanova, E., Fehsenfeld, S., Mantamadiotis, T., Lemberger, T., Greiner, E., Stewart, A. F., and Schütz, G. (2001). A CamKIIalpha iCre BAC allows brain-specific gene inactivation. *Genesis*, 31(1):37-42. doi:10.1002/gene.1078.
- Chen, C. T. (2019). Employing CRISPR/Cas9 Techniques to Knockout A-type Potassium Channel in Hippocampus neurons. Unpublished master's thesis. National Taiwan University. doi:10.6342/NTU201903709
- Chen, X. X., Yuan, L. L., Zhao, C. P., Birnbaum, S. G., . . . Johnston, D. (2006). Deletion of Kv4.2 Gene Eliminates Dendritic A-Type K⁺ Current and Enhances Induction of Long-Term Potentiation in Hippocampal CA1 Pyramidal Neurons. *J Neurosci*, 26(47):12143-12151. Doi:10.1523/JNEUROSCI.2667-06.2006
- Choe, S. (2002). Potassium channel structures. *Nat Rev Neurosci.*, 3(2):115-21.
Doi:10.1038/nrn727
- Clark, B. D., Kwon, E., Maffie, J., Jeong, H. Y., Nadal, M., Strop, P. and Rudy, B. (2008). DPP6 Localization in Brain Supports Function as a Kv4 Channel Associated Protein. *Front. Mol. Neurosci.*, 1(8). doi:10.3389/neuro.02.008.2008
- Coetzee, W. A., Amarillo, Y., Chiu, J., Chow, A., . . . Rudy, B. (1999). Molecular diversity of K⁺ channels. *Ann N Y Acad Sci.*, 868:233-85.
Doi:10.1111/j.1749-6332.1999.tb11293.x
- Guidelli, R. (2020). The common features of tetrameric ion channels and the role of electrostatic interactions. *Electrochem Commun.*, 121.
Doi:10.1016/j.elecom.2020.106886
- Guo, W. N., Jung, W. E., Marionneau, C., Aimond, F., . . . and Nerbonne, J. M. (2005).

- 
- Targeted deletion of Kv4.2 eliminates I(to,f) and results in electrical and molecular remodeling, with no evidence of ventricular hypertrophy or myocardial dysfunction. *Circ Res*, 97(12):1342-50. Doi:10.1161/01.RES.0000196559.63223.aa
- Heginbotham, L., Lu, Z., Abramson, T., and MacKinnon, R. (1994). Mutations in the K⁺ channel signature sequence. *Biophys J.*, 66:1061–1067. doi: 10.1016/S0006-3495(94)80887-2
- Hu, H. J., Carrasquillo, Y., Karim F., . . . and Schwarz, T. L. (2006). The Kv4.2 Potassium Channel Subunit Is Required for Pain Plasticity. *Neuron*, 50(1):89-100. Doi:10.1016/j.neuron.2006.03.010
- Hu, H. J., Carrasquillo, Y., Karim, F., Jung, W. E., Nerbone, J. M., Schwarz, T. L. and Robert, W. G. 4th. (2006). The kv4.2 potassium channel subunit is required for pain plasticity. *Neuron*, 50(1), 89-100. doi: 10.1016/j.neuron.2006.03.010.
- Hu, J. H., Malloy, C., Tabor, G. T., Gutzmann, J. J., Liu, Y., Abebe, D., Karlsson, R. M., Durell, S., Cameron, H. A. and Hoffman, D. A. (2020). Activity-dependent isomerization of Kv4.2 by Pin1 regulates cognitive flexibility. *Nat Commun*, 11(1), doi: 10.1038/s41467-020-15390-x
- Jung, S. C., Kin, J., and Hoffman, D. A. (2008). Rapid, Bidirectional Remodeling of Synaptic NMDA Receptor Subunit Composition by A-type K⁺ Channel Activity in Hippocampal CA1 Pyramidal Neurons. *Neuron*, 60(4), 657-671. doi: 10.1016/j.neuron.2008.08.029
- Kim, D. M., and Nimigean, C. M. (2016). Voltage-Gated Potassium Channels: A Structural Examination of Selectivity and Gating. *Cold Spring Harb Perspect Biol.*, 8(5):a029231. Doi:10.1101/cshperspect.a02931
- Kim, J., Jung, S. C., Clemens, A. M., Petralia, R. S. and Hoffman D. A. (2007). Regulation of dendritic excitability by activity-dependent trafficking of the A-type K⁺ channel subunit Kv4.2 in hippocampal neurons. *Neuron*, 54(6), 933-947. doi:10:1016/j.neuron.2007.05.026
- Kuang, Q., Purhonen, P., and Hebert, H. (2015). Structure of potassium channels. *Cell Mo Life Sci.*, 72:3677-3693. Doi:10.1007/s00018-015-1948-5
- Lee, H. Y., Ge, W. P., Huang, W., He, Y., Wang, G. X., Rowson-Baldwin, A., Smith, S. J., Jan, Y. N., and Jan, L. Y. (2011). Bidirectional Regulation of Dendritic Voltage-Gated Potassium Channels by the Fragile X Mental Retardation Protein. *Neuron*, 72(4), 630-642. doi:10.1016/j.neuron.2011.09.033
- Liu, Y. Q., Huang, W. X., Sanchez, R. M., Min, J. W., Hu, J. J., He, X. H., and Peng, B. W. (2014). Regulation of Kv4.2 A-type potassium channels in HEK-293 cells by hypoxia. *Front. Cell. Neurosci.* 14. doi: 10.3389/fncel.2014.00329.
- Lockridge, A., Su, J., Yuan, L. L. (2010). Abnormal 5-HT modulation of stress behaviors in the Kv4.2 knockout mouse. *Neuroscience*. 170(4), 1086-1087. doi:

- 10.1016/j.neuriscience.2010.08.047
- Menegola, M., Clark, E., and Trimmer, J. S. (2012). The importance of immunohistochemical analyses in evaluating the phenotype of Kv channel knockout mice. *Epilepsia*, 53(Suppl 1):142-9. Doi:10.1111/j.1528-1167.2012.03485.x
- Menegola, M., Clark, E., and Trimmer, J. S. (2012). The Importance of Immunohistochemical Analyses in Evaluating the Phenotype of Kv Channel Knockout Mice. *Epilepsia*, 53(Suppl 1):142-149. Doi:10.1111/j.1528-1167.2012.03485.x
- Migliore, M., Ferrante, M., Ascoli, G. A. (2005). Signal propagation in oblique dendrites of CA1 pyramidal cells. *J Neurophysiol*. 94(6):4145-55. doi: 10.1152/jn.00521.2005.
- Miller, C. (2000). An overview of the potassium channel family. *Genome Biol.*, 1(4). Doi:10.1186/gb-2000-1-4-reviews0004
- Min, M. Y., Wu, Y. W., Shih, P. Y., Lu, H. W., Wu, Y., and Hsu, C. L. (2010). Roles of A-type potassium currents in tuning spike frequency and integrating synaptic transmission in noradrenergic neurons of the A7 catecholamine cell group in rats. *Neuroscience*, 168(3):633–45
- Nerbonne, J. M., Gerber, B. R., Norris, A., and Burkhalter, A. (2008). Electrical remodelling maintains firing properties in cortical pyramidal neurons lacking KCND2-encoded A-type K⁺ currents. *J Physiol*, 586(Pt 6):1565-1579. Doi:10.1113/jphysiol.2007.146597
- Oh, M. M., Simkin, D., and Disterhoft, J. F. (2016). Intrinsic Hippocampal Excitability Changes of Opposite Signs and Different Origins in CA1 and CA3 Pyramidal Neurons Underlie Aging-Related Cognitive Deficits. *Front Syst Neurosci*, 10(52). doi: 10.3389/fnsys.2016.00052
- Platt, R. J., Chen, S., Zhou, Y., Yim, M. J., Sweich, L., Kempton, H. R., Zhang, F. (2014). CRISPR-Cas9 Knockin Mice for Genome Editing and Cancer Modeling. *Cell*, 159(2), 440-455. doi: 10.1016/j.cell.2014.09.014
- Qu, J., Mulo, I., and Myhr, K. L. (2009). The development of Kv4.2 expression in the retina. *Neurosci Lett*, 464(3):209-13. Doi:10.1016/j.neulet.2009.08.048
- Ranjan, R., Logette, E., Marani, M., Herzog, M., . . . Markram, H. (2019). A Kinetic Map of the Homomeric Voltage-Gated Potassium Channel (Kv) Family. *Front Cell Neurosci*. doi:10.3389/fncel.2019.00358
- Rhodes, K. J., Carroll, K. I., Sung, M. A., Doliveira, L. C., . . . Trimmer, J. S. (2004). KChIPs and Kv4 alpha subunits as integral components of A-type potassium channels in mammalian brain. *J Neurosci*, 24(36):7903-15. Doi:10.1523/JNEUROSCI.0776-04-2004
- Seikel, E., and Trimmer, J. S. (2009). Convergent modulation of Kv4.2 channel alpha

- 
- subunits by structurally distinct DPPX and KChIP auxiliary subunits. *Biochemistry*, 48(24):5721-30. Doi:10.1021/bi802316m
- Simkin, D., Hattori, S., Ybarra, N., Musial, T. M., Buss, E. W., Richter, H., Oh, M. M., Nicholson, D. A. and Disterhoft, J. F. (2015). Aging-Related Hyperexcitability in CA3 Pyramidal Neurons Is Mediated by Enhanced A-Type K⁺ Channel Function and Expression. *J Neurosci*, 35(38):13206-13218. doi: 10.1523/JNEUROSCI.0193-15.2015
- Storm, J. F. (1990). Potassium currents in hippocampal pyramidal cells. *Prog Brain Res*, 83:161-87. Doi:10.1016/s0079-6123(08)61248-0
- Wu, R. N., Hung, W. C., . . . Wong, S. B. (2020). Firing activity of locus coeruleus noradrenergic neurons decreases in necdin-deficient mice, an animal model of Prader–Willi syndrome. *J Neurodev Disord*, 12(21). Doi:10.1186/s11689-020-093234
- Zhang, Y. Q., Tachtsidis, G., Schob, C., Koko, M., . . . Bähring, R. (2021). KCND2 variants associated with global developmental delay differentially impair Kv4.2 channel gating. *Hum Mol Genet*, 30(23):2300-2314. Doi:10.1093/hmg/ddab192

Chapter 6. Figures and Legends

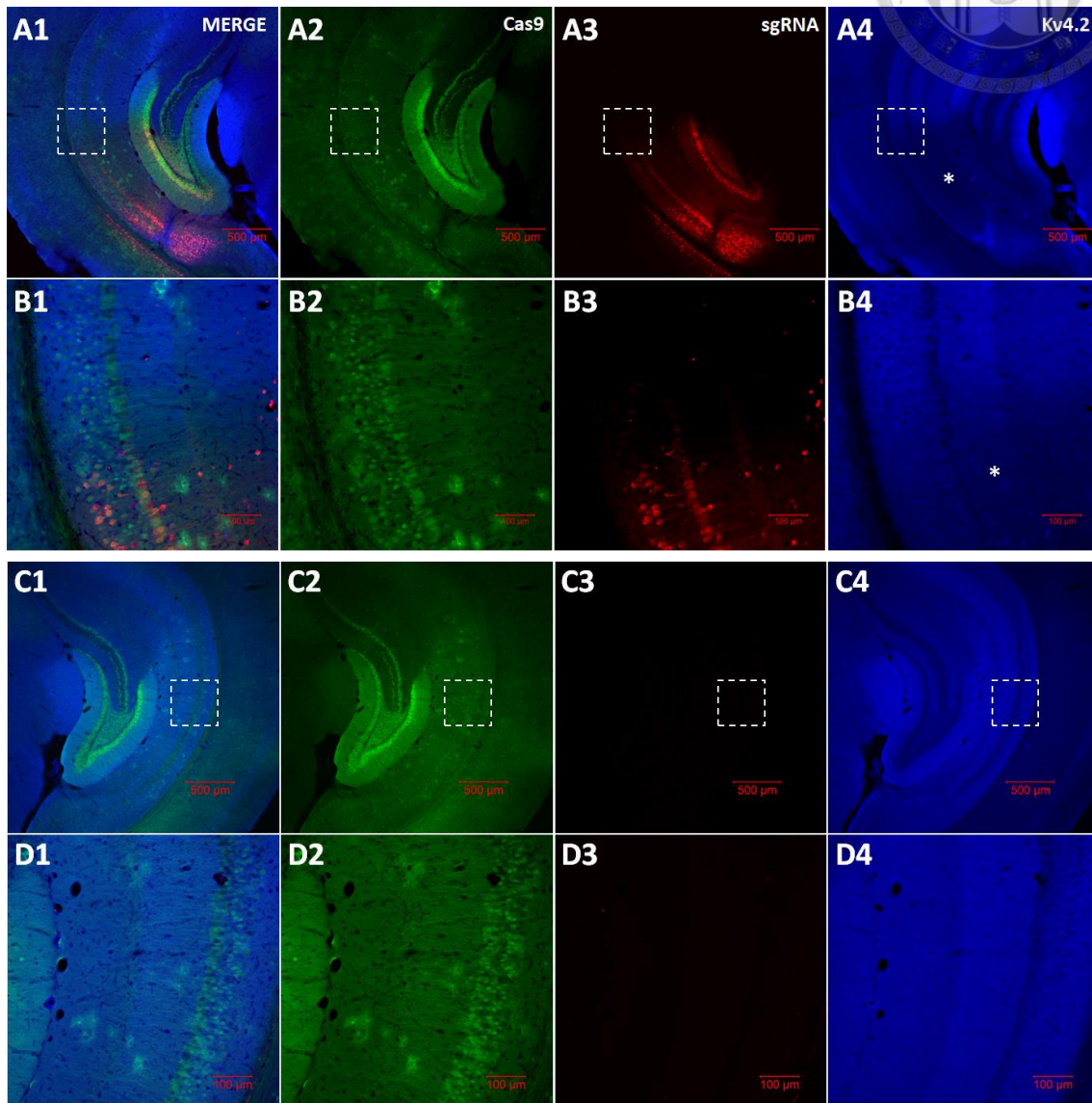


Figure 1. Genomic editing of Kv4.2 by Kv4.2 KO system.

Kv4.2 KO sgRNA was injected to one side of hippocampus in *cas9*^{CamKII α -iCre} mouse. Lower Kv4.2-ir was observed in the regions expressing both KO sgRNAs as well as cas9 on ipsilateral side of virus infection (A, B) compared to contralateral side (C,D), indicated as asterisk sign. GFP signals indicated cas9 protein expression. Mcherry signals indicated sgRNAs expression. Kv4.2 was stained by DyLight 405 fluorescence. B,D presented a higher magnification of the dashed-square in A,B. All pictures were taken under 4X (A, C) and 20X (B, D) lens of confocal imaging.

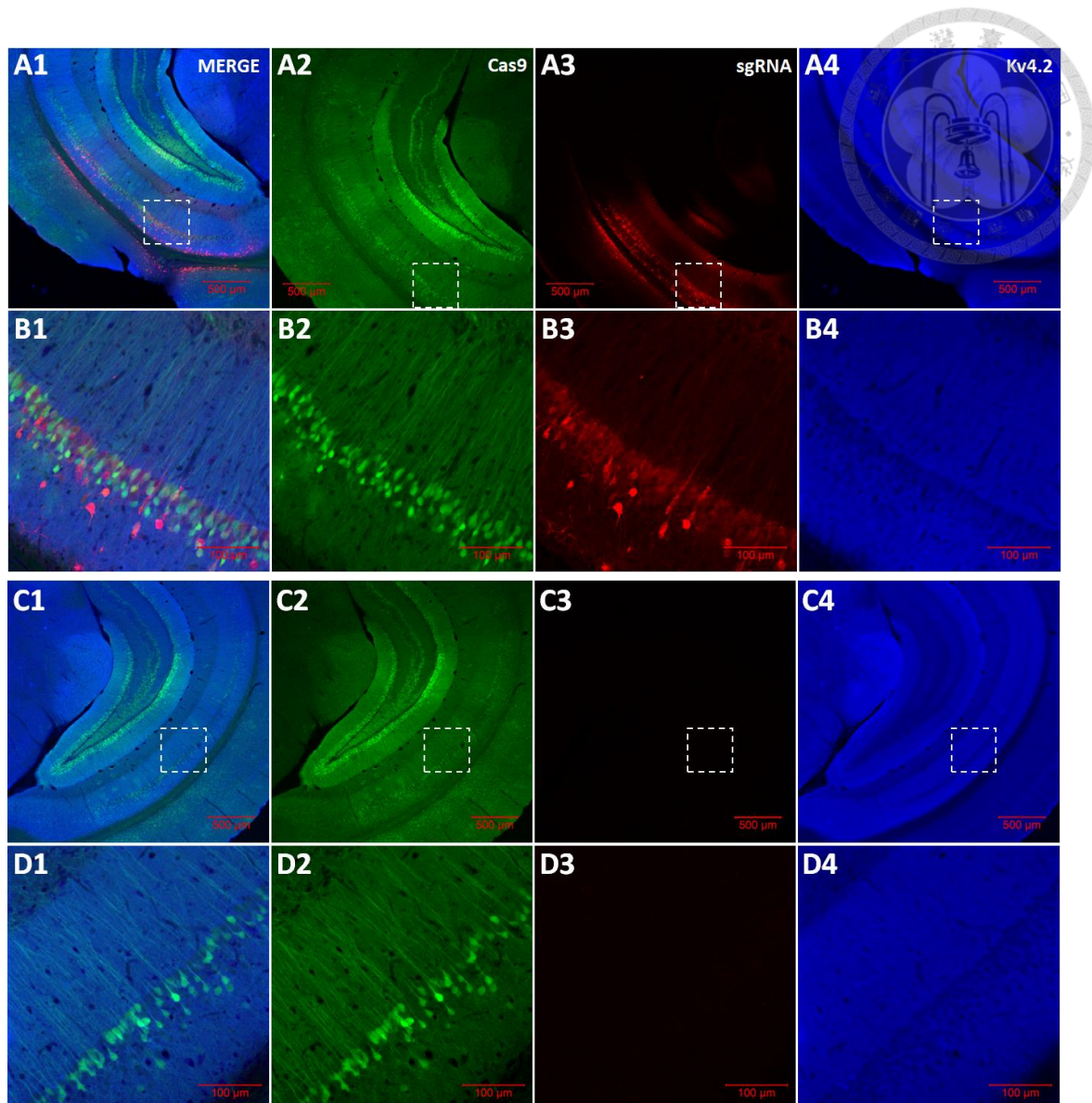


Figure 2. Genomic editing of Kv4.2 by Kv4.2 control virus system infection.

Kv4.2 control sgRNA was injected to one side of hippocampus in $cas9^{CamKII\alpha-iCre}$ mouse. Lower Kv4.2-ir was observed in the regions expressing both KO sgRNAs as well as cas9 on ipsilateral side of virus infection (A, B) compared to contralateral side (C,D). GFP signals indicated cas9 protein expression. Mcherry signals indicated sgRNAs expression. Kv4.2 was stained by DyLight 405 fluorescence. B,D presented a higher magnification of the dashed-square in A,B. All pictures were taken under 4X (A, C) and 20X (B, D) lens of confocal imaging.

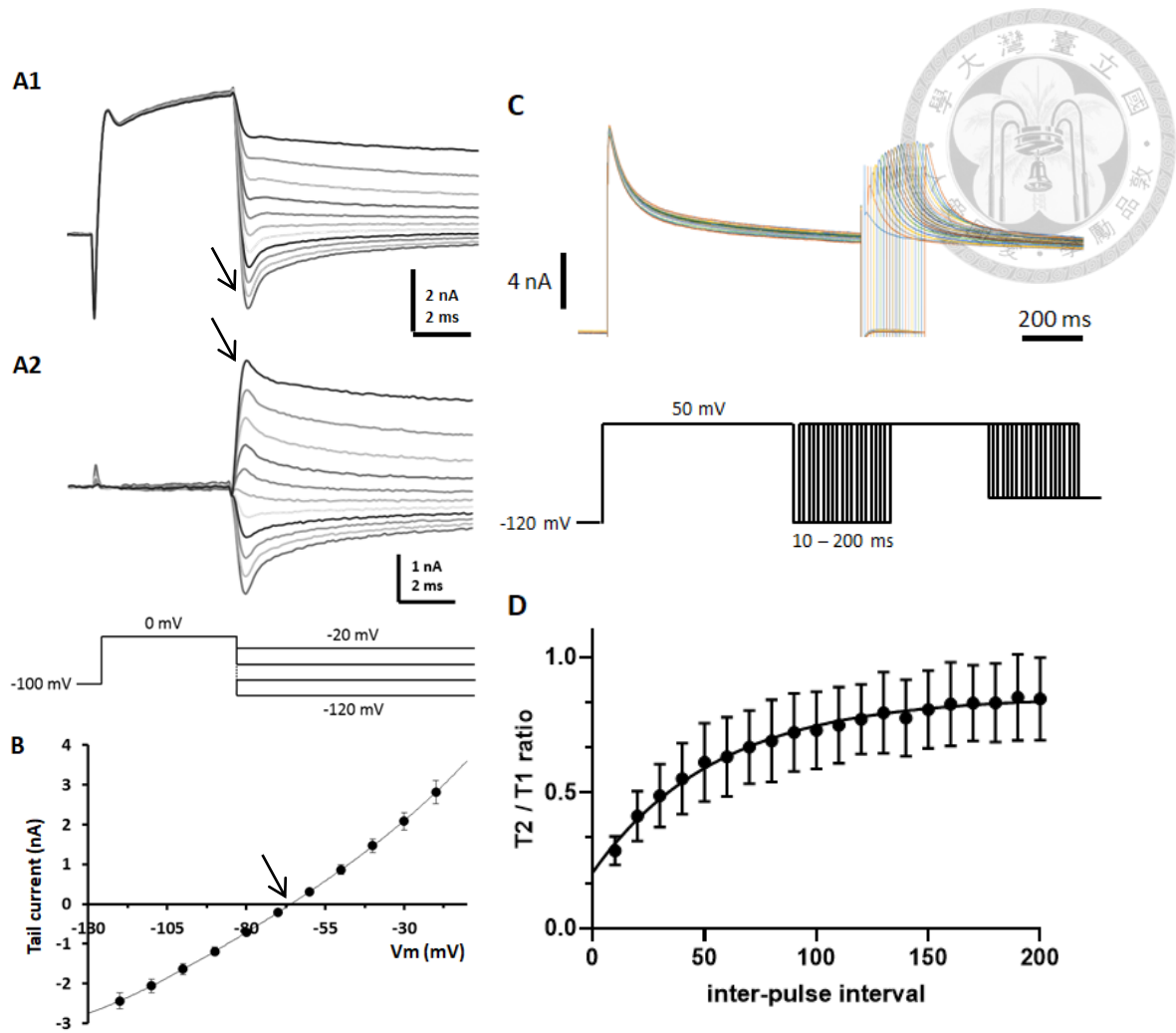


Figure 3. Reversal potential and recovery time of fast-activating potassium channels. (A) Superimposed tail currents of fast-activating potassium channels before (A1) and after (A2) leak subtraction, indicated as arrow. Tail currents were evoked by voltage steps from -100 to 0 mV (5 ms), followed to a level ranging from -20 to -120 mV with 10 mV increments (lower traces). The peak amplitude of tail currents was measured and plotted versus voltage level (B), which were summarized from 5 CA1 pyramidal neurons. Data were fitted to a quadratic polynomial equation (solid line). Reversal potential was calculated as the imaginative voltage where tail current = 0 , indicated as arrow. (C) Superimposed fast-activating potassium currents evoked by paired voltage pulses from -120 to $+50$ mV with various inter-pulse intervals from 10 to 200 ms with a 10 ms increment (lower traces). (D) The curve of recovery from inactivation summarized from 3 CA1 pyramidal neurons. The solid line shows the results of fitting single exponential growth to the data.

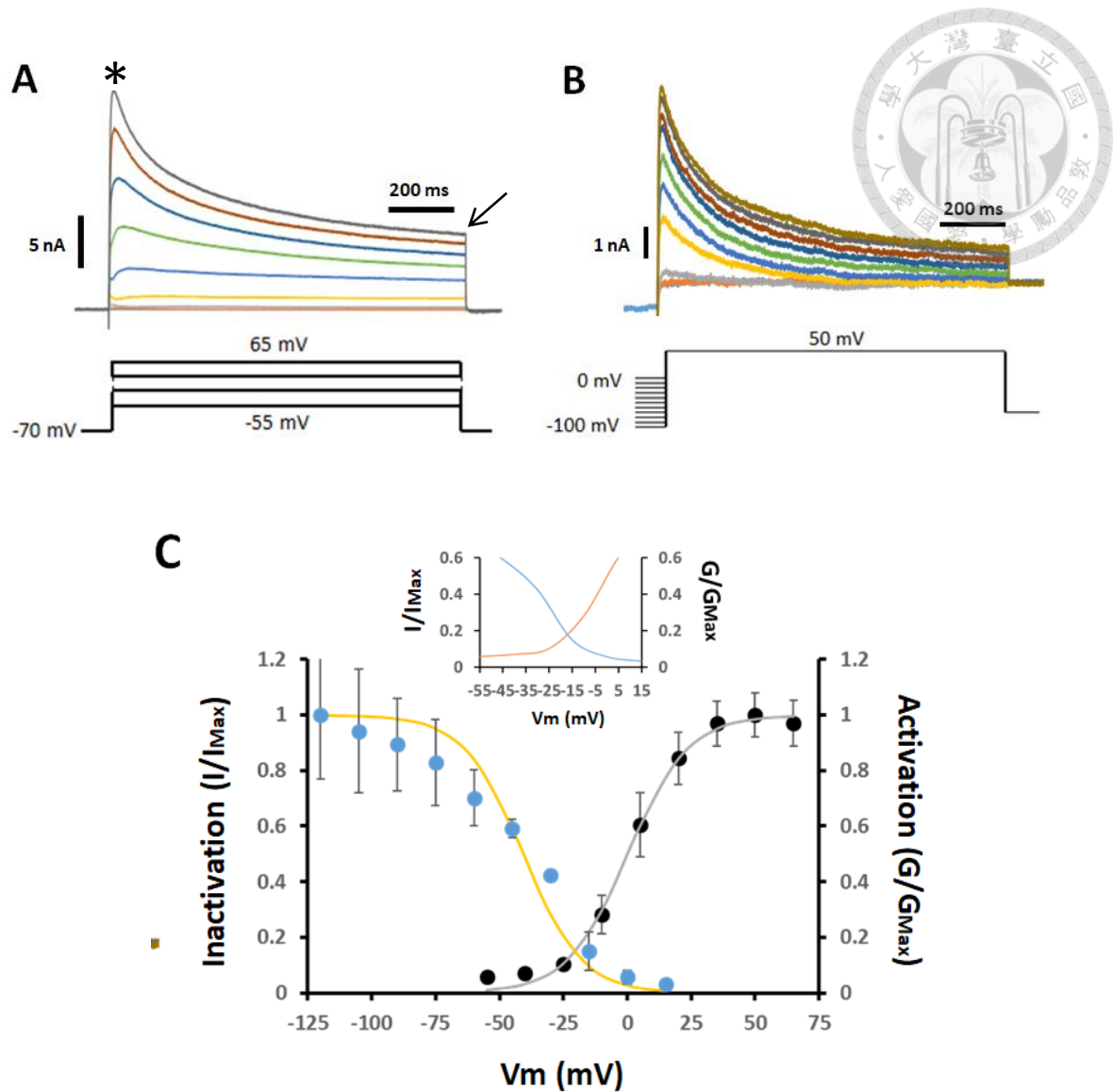


Figure 4. Activation and inactivation of fast-activating potassium channels.

(A) Superimposed I_K evoked in a CA1 pyramidal neuron (upper traces). The whole-cell I_K were evoked by voltage steps from -55 to $+65$ mV with a 15 mV increment (lower traces). (B) Superimposed I_K (upper traces) evoked by voltage steps from various pre-pulse voltage levels (-100 to 0 mV with a 10 mV increment) (lower traces) to 50 mV. (C) The activation (black circles + grey line)/inactivation (blue circles + yellow line) curve for the I_K , summarized from 18 and 2 CA1 pyramidal neurons, respectively. Note the overlapping of the two curves between V_m of -55 and 15 mV, as shown in the insert. The solid lines were obtained by fitting the Boltzmann's equation to the data.

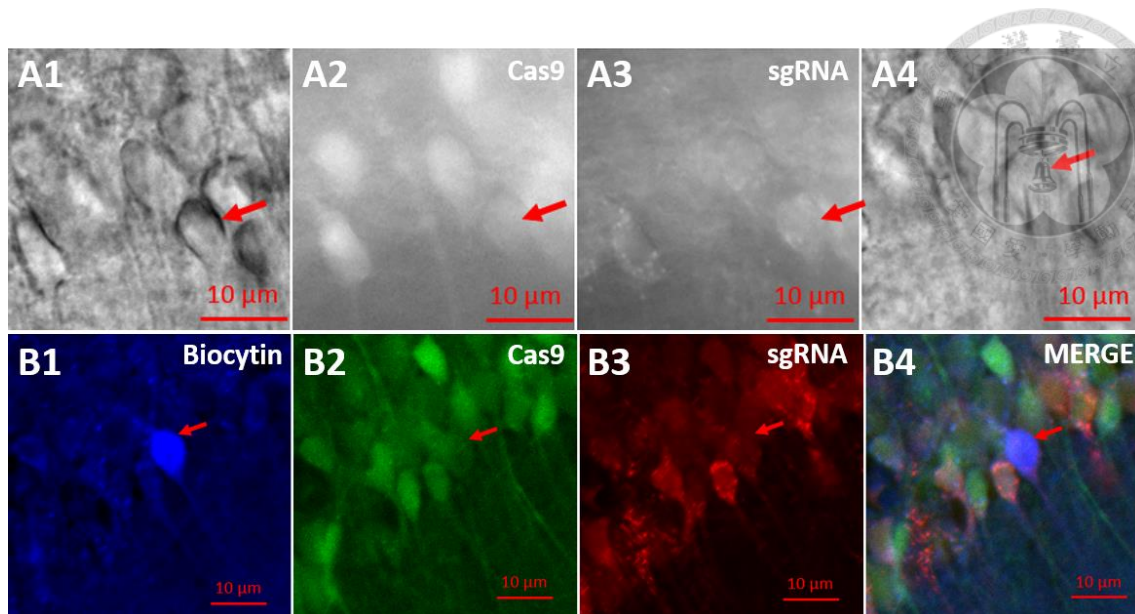


Figure 5. Recordings from, and post-hoc examination of, Kv4.2 KO or CTRL virus group of CA1 pyramidal neurons.

Cas9 (A2) and sgRNAs (A3) expression of CA1 pyramidal neurons were observed under IR-DIC microscope before recordings. Neurons expressing both fluorescent signals will be counted as KO group or CTRL virus group, depending on which virus being injected. Neural morphology before (A1) and during (A4) recording were shown. Neurons will be filled with biocytin during recording and saved in 4% PFA for post-hoc examination. Cell type of recorded neurons was observed by biocytin-ir (B1). Cells that were not pyramidal neurons would be excluded. Cas9 (B2) and sgRNAs (B3) expression were observed in KO group or CTRL virus group (B) as supportive data. Merge of 3 signals (B4) were shown.

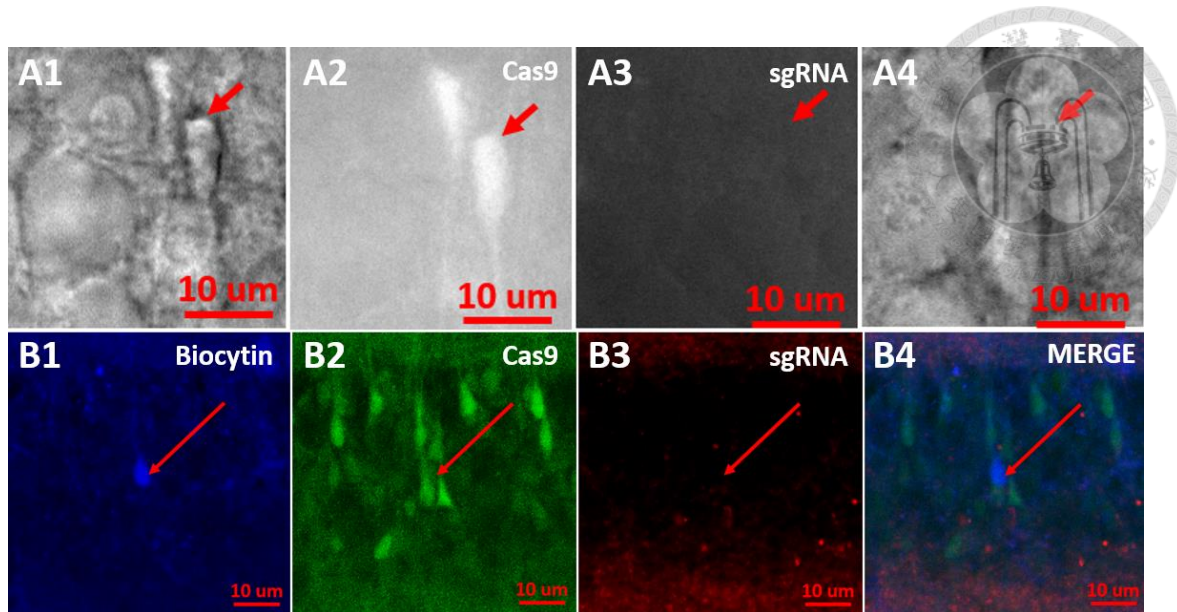


Figure 6. Recordings from, and post-hoc examination of, Kv4.2 CTRL group of CA1 pyramidal neurons.

Cas9 (A2) and sgRNAs (A3) expression of CA1 pyramidal neurons were observed under IR-DIC microscope before recordings. Neurons that didn't expressing both fluorescent signals will be counted as CTRL group. Neural morphology before (A1) and during (A4) recording were shown. Neurons will be filled with biocytin during recording and saved in 4% PFA for post-hoc examination. Cell type of recorded neurons was observed by biocytin-ir (B1). Cells that were not pyramidal neurons would be excluded. Either Cas9 (B2) or sgRNAs (B3) expression was not observed in CTRL group as supportive data. Merge of 3 signals (B4) were shown.

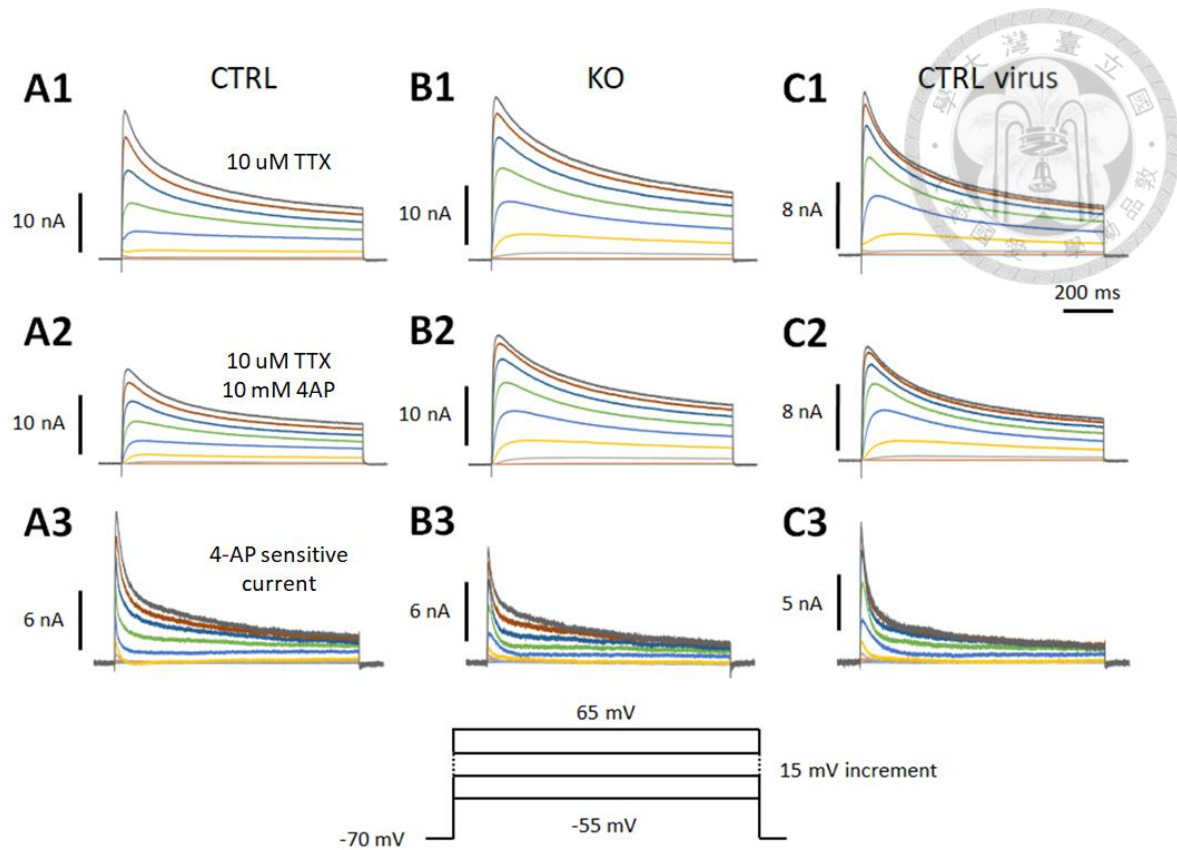


Figure 7. Depolarization induced outward currents of Kv4.2 KO and control groups in CA1 pyramidal neurons.

Superimposed I_K evoked in CTRL group (A1), KO group (B1), and CTRL virus group (C1). The whole-cell I_K were evoked by voltage steps from -55 to $+65$ mV with a 15 mV increment (lower traces). 10 mM 4-AP was applied later at the same cell (A2-C2). 4-AP sensitive current was generated from subtraction of I_K after by before 4-AP application (A3-C3).

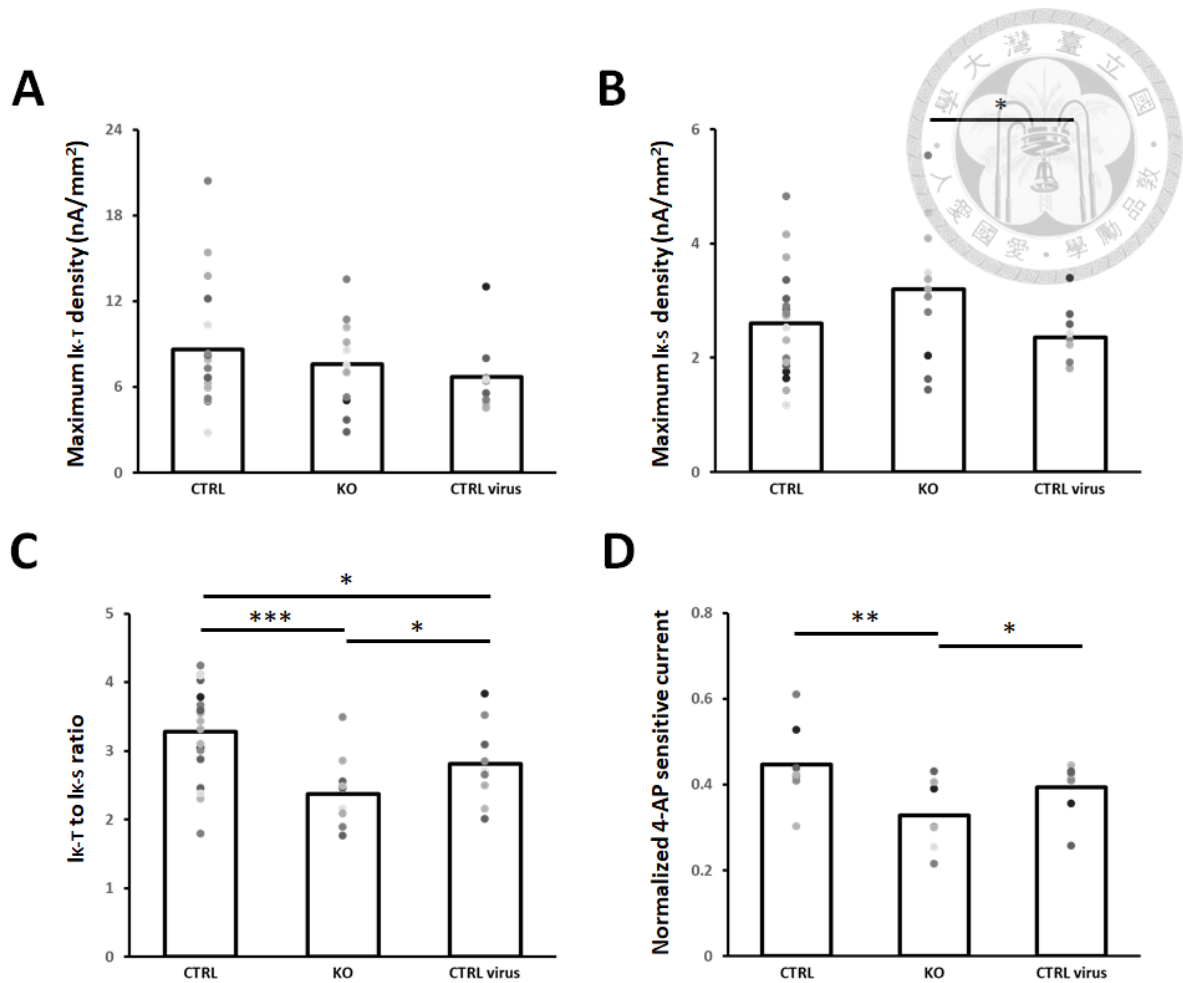


Figure 8. The I_A are attenuated in Kv4.2 KO group.

(A) Maximum I_{K-T} density showed no difference in CTRL group (N=18), KO group (N=11) and CTRL virus group (N=9). (B) Maximum I_{K-S} density t density showed significant difference in KO group (N=11) compared to CTRL virus group (N=9), but no difference compared to CTRL group (N=18). (C) I_{K-T} to I_{K-S} ratio was significantly decreased in KO group (N=19) compared to CTRL group (N=11) and CTRL virus group (N=9). (D) Normalized 4-AP sensitive current was significantly decreased in KO group (N=7) compared to CTRL group (N=8) and CTRL virus group (N=8). Asterisks denote * $p < 0.05$, ** $p < 0.01$ and *** $p < 0.001$.